Supporting Information

Miranda et al. 10.1073/pnas.1219611110

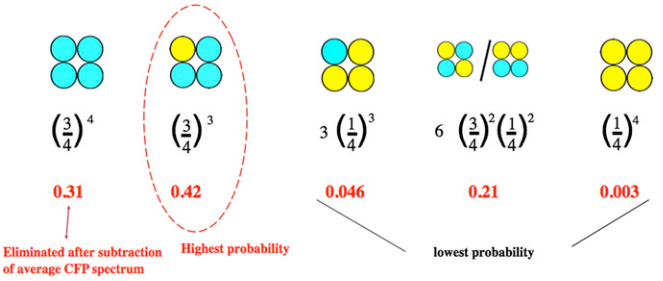

Fig. S1. Subunit combinations forming the heterotetramers. Quantified RNA was injected with CFP-tagged and YFP-tagged BK in a 3:1 ratio. Assuming both RNA types are processed with the same efficiency by the oocyte, it is expected that the probability of tetramer composition follows a binomial distribution given by the expression $p_i = P_Y^i P_C^{n-i}\binom{i}{n}$, where p_i is the probability of i YFP subunits, $n = 4$, and P_Y and P_C are the probabilities of encountering a CFP- or YFP-tagged subunit in the total protein pool, here assumed to be 1/4 and 3/4, respectively. Probabilities of different tetramers are shown below for each possible combination. Highest probabilities are for the 3CFP:1YFP heterotetramer and for the 4CFP homotetramer. Fluorescence from the latter does not contribute to the FRET signal measured.

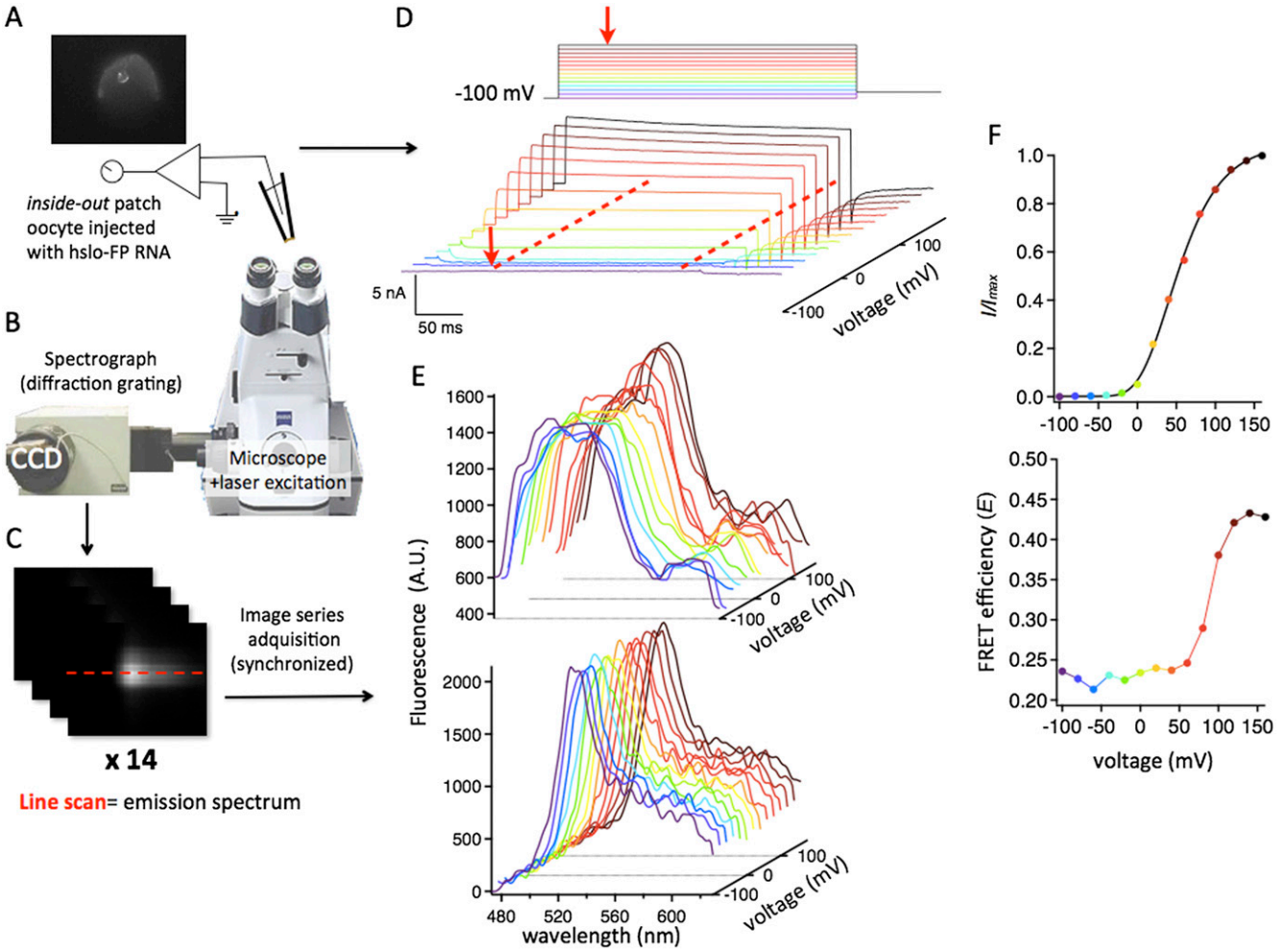

Fig. S2. Spectral-FRET recording from BK channels in membrane patches. (*A*) Inside-out patches are excised from *Xenopus* oocytes microinjected with cRNA combinations of fluorescent large-conductance voltage- and calcium- dependent (BK) channel constructs. Light from the patch is diffracted through the spectrograph (*B*) onto the CCD camera, to obtain spectral images of the patch (*C*). Synchronous optical and electrical recordings show a series of currents (*D*) and spectra (*E*) color-coded according to the voltage steps (−100 to +160 mV). Representative recordings from the construct BK-667YC in 12 μM Ca^{2+} are shown. Spectra (*Upper*, 458-nm excitation, CFP+FRET-YFP; *Lower*, 488-nm excitation, YFP alone) were recorded during steady-state current pulses (red arrow and dashed lines). (*F*) Normalized tail current (*Upper*; proportional to open probability) and FRET efficiency (*E*; *Methods* and Fig. S3) show remarkably similar voltage dependence.

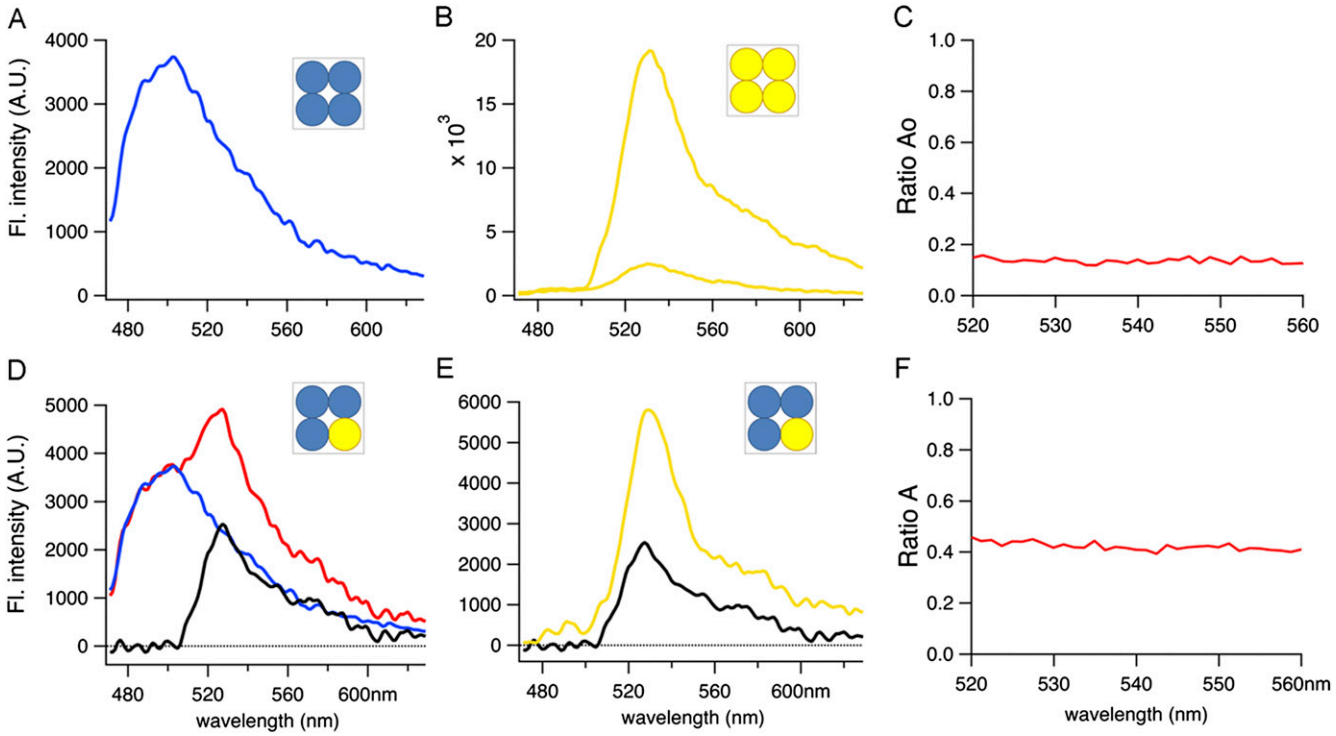

Fig. S3. Spectral analysis procedure. (*A*) Normalized CFP spectrum is obtained as an average from 10 patches expressing BK-CFP. (*B*) Two emission spectra of patches expressing BK-YFP constructs are obtained after excitation at 458 and 488 nm, which are the excitation wavelengths for CFP and YFP, respectively. The 458-nm light does provide some residual excitation of YFP as shown by the lower curve. (*C*) Ratio calculation between spectra in *B* yields the $RatioA_0$ values, which accounts for the direct (no-FRET) YFP excitation. (*D*) The red line represents the spectrum of a patch expressing CFP/YFP combinations. The normalized CFP spectrum (blue line) is first fitted and subtracted. The resulting spectrum (black line) is a combination of direct excitation of YFP at 458 nm plus excitation of YFP by FRET. Finally, this spectrum is compared with the spectrum of the same patch at 488-nm excitation (*E*), which yields RatioA values (*F*). RatioA and $RatioA_0$ are used to calculate the normalized FRET efficiency *E* (*Methods*) (1, 2).

1. Zheng J, Zagotta WN (2003) Patch-clamp fluorometry recording of conformational rearrangements of ion channels. *Sci STKE* 2003(176):PL7.
2. Zheng J, Varnum MD, Zagotta WN (2003) Disruption of an intersubunit interaction underlies Ca^{2+}-calmodulin modulation of cyclic nucleotide-gated channels. *J Neurosci* 23(22): 8167–8175.

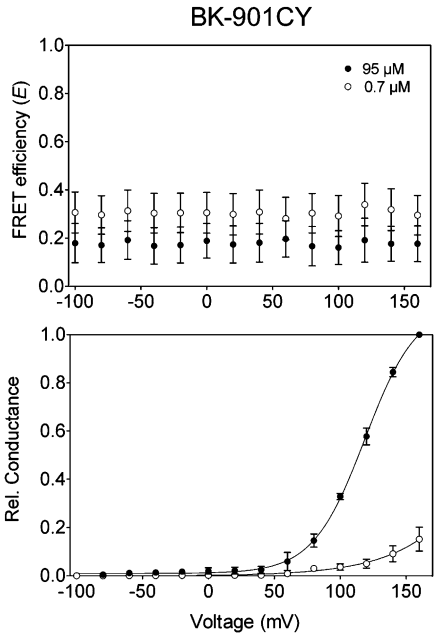

Fig. S4. Patch-clamp fluorometry recording of BK-901 construct. *E–V* (*Upper*) and *G–V* curves (*Lower*) were determined from simultaneous recording of currents and spectra from patches expressing BK-901CY heterotetramers. Data points and error bars represent averages ± SEM ($n = 6$). Ca^{2+} concentrations are indicated in the legend.

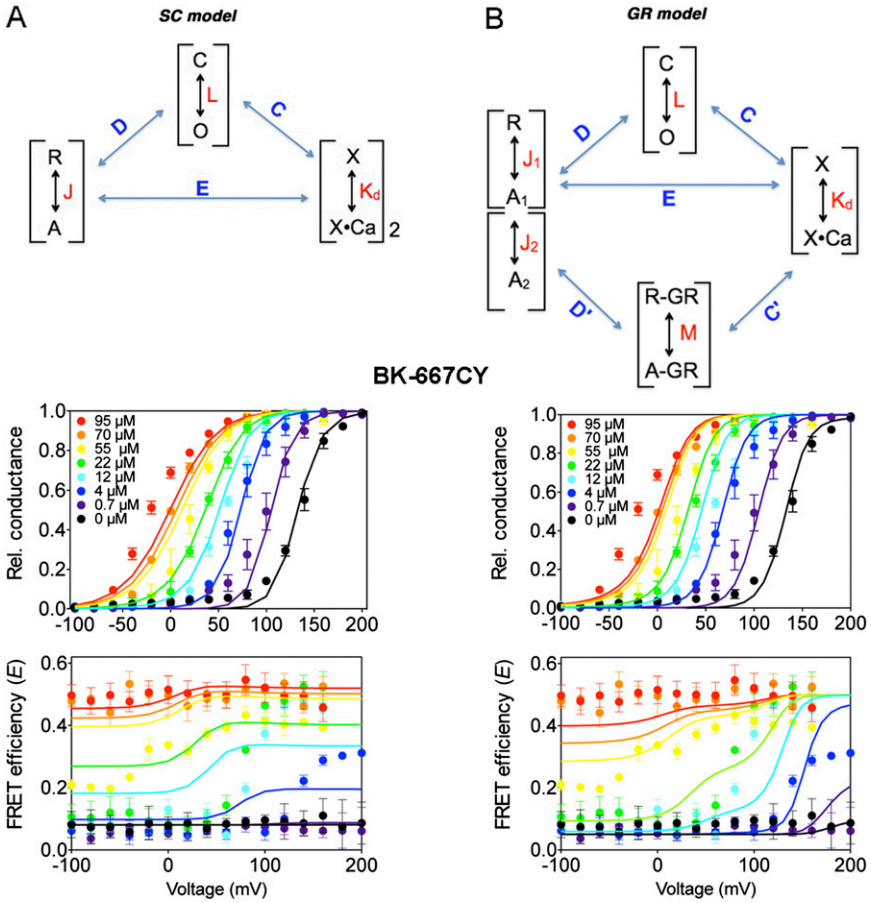

Fig. S5. Simultaneous fitting of gating and FRET signals. (*A*, *Upper*) Sweet and Cox (1) model, which was used to fit the *G–V* curves in Figs. 3*A* and 4*A*. In each subunit, two calcium binding sites are coupled to the resting↔activated transition of a voltage sensor (allosteric constant *E*), and each of these is coupled to the concerted closed↔open transition for the ion channel (allosteric constants *C* and *D*). (*A*, *Lower*) Application of this model (solid curves) to simultaneously describe the *G–V* and *E–V* data obtained in this study. Whereas *G–V* curves are well fitted using this model, it does not correctly predict the *E–V* data. The steady-state parameters that give rise to the solid curves are V_h (*J*) = 148 mV, $z_J = 0.58$ e, $L_0 = 2.2 \times 10^{-6}$, $z_L = 0.42$ e, $K_{d1} = 4.1$ μM, $K_{d2} = 39$ μM, $C_1 = 3.6$, $C_2 = 6.16$, $D = 30.4$, $E_1 = 1$, $E_2 = 2.1$, where *J, K*, and *L* are the equilibrium constants for voltage sensor activation, Ca^{2+} binding, and C-O transition, respectively; V_h (J) is the voltage where $J = 1$; L_0 and z_J are the zero voltage value of *L* and its partial charge, respectively; K_{d1} and K_{d2} are the Ca^{2+} dissociation constants, and C_1, C_2, *D*, E_1, and E_2 are the allosteric constants describing channel opening/Ca^{2+} binding, channel opening/voltage sensor activation, and voltage sensor activation/Ca^{2+} binding interactions, respectively (1, 2). (*B*) An example showing our attempts to modify the allosteric model to fit our results. In this example (*Upper*), we assumed that each of the four voltage sensor domains, once activated, can undergo a "relaxation" step, as has been seen in various S4-type voltage sensors (3), but for which there is no evidence currently for the BK channel. Whereas the first transition (equilibrium constant J_1) is coupled to Ca^{2+} binding and channel opening (allosteric constants *D* and *E*), the second transition (equilibrium constant J_2) is coupled to a concerted conformational change of the gating ring (GR) that has a basic equilibrium constant *M*. It is the probability p_A of this activated state that affects FRET efficiency. For every voltage sensor in state A_2 and every binding site with Ca^{2+} bound, the GR equilibrium is increased by the factors *D′* and *C′*, respectively. Although this model gave the best description of those we tried, it predicts complicated gating currents and more work is required to investigate how well these predictions correspond to the actual biophysical properties of the BK channel. (*B*, *Lower*) Description of the Ca^{2+} and voltage dependence of both the channel opening and the FRET signal (solid lines) provided with the scheme *B* expanded to include two Ca^{2+} binding sites in each subunit. The parameter values that give rise to the curves in *B* are as follows: $V_h(J_1)$ = 148 mV, $V_h(J_2)$ = 160 mV, $z_{J1} = 0.58$ e, $z_{J2} = 1.5$ e, $K_{d1} = 4$ μM, $K_{d2} = 100$ μM, $L_0 = 5.41 \times 10^{-6}$, $z_L = 0.41$ e, $C_1 = 6.12$, $C_2 = 1.92$, $D = 25$, $E_1 = 1$, $E_2 = 1.2$, $C_1' = 1.33$, $C_2' = 20.2$, $D' = 6$, and $M = 0.0001$. Modeling methods: Calculation of the open probability and the energy transfer efficiency for a wide range of models was done with a MATLAB program that could include multiple concerted transitions, binding sites, and voltage sensors. In a brute-force approach, we used matrix algebra to compute the partition function and thereby the probability of each state for a given Ca^{2+} concentration and membrane potential. Through various optimizations, we were able to work with models having more than 2^{20} states. The sum of the probabilities of the states in which the channel is open provided the open probability values, which were compared with *G–V* data. For the models shown here, the underlying FRET changes assumed only two values, *E* was obtained as $E = E_R + p_A(E_A - E_R)$, where E_R is the resting FRET efficiency, E_A is the active-state efficiency, and p_A is the probability of active states at a given voltage and calcium concentration.

1. Sweet T-B, Cox DH (2008) Measurements of the BKCa channel's high-affinity Ca^{2+} binding constants: Effects of membrane voltage. *J Gen Physiol* 132(5):491–505.
2. Horrigan FT, Aldrich RW (2002) Coupling between voltage sensor activation, Ca^{2+} binding and channel opening in large conductance (BK) potassium channels. *J Gen Physiol* 120(3): 267–305.
3. Villalba-Galea CA, Sandtner W, Starace DM, Bezanilla F (2008) S4-based voltage sensors have three major conformations. *Proc Natl Acad Sci USA* 105(46):17600–17607.

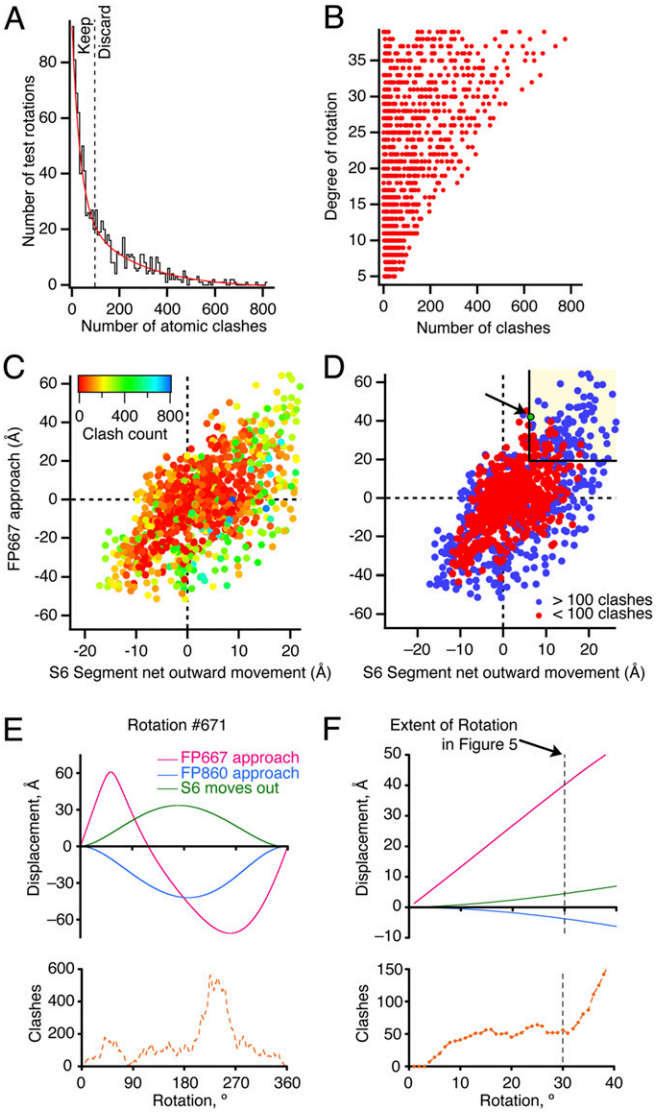

Fig. S6. Statistics of candidate models for gating-ring motion. (*A*) The distribution of 1,000 models formed by random rotations of gating-ring subunits. The histogram shows the number of atomic clashes (proximity, <2.2 Å). Clashes between two immediately adjacent subunits (~10,000 atoms) were assessed. Many models had few clashes, and the cutoff (dashed line) was set at 100 clashes, or about 1% of the total atoms considered. (*B*) The number of clashes for the 1,000 models plotted against the magnitude of rotation, in degrees. All rotation extents gave some models with a small number of clashes, but large, physically nonsensical clash counts only occurred for large rotations. (*C*) For each model is plotted the expected approach of the fluorescent proteins inserted at 667, and the expected movement of the S6 segment. The color of each point represents the count of clashes. (*D*) Simplified version of *C*, showing the models with less than 100 clashes as red dots. Only 26 models sit in the shaded area for which the gate moved >6 Å, and the approach of the fluorescent proteins was >20 Å. Most of these models were implausible as they either (*i*) brought the 860 insertions much closer together, opposite to the FRET signal we observed, or (*ii*) were only reached following substantial clashes during the rotation. Relative position of model shown in Fig. 5 (*Right*) is indicated with a green circle and arrow. (*E*) Clashes, fluorophore positions, and S6 linker of a full 360° rotation of the each subunit around the axis used to generate the model in Fig. 5. Steric clashes between fluorophores were not assessed, and 30° rotation brought the insertions at 667 to their closest possible extent. (*F*) Same plot as *E* but on an expanded scale.

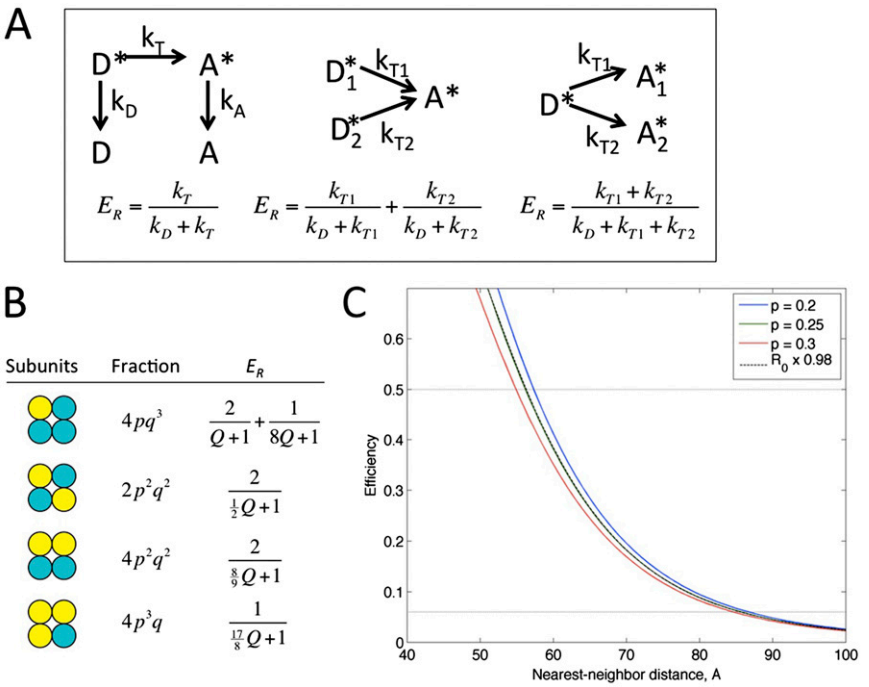

Fig. S7. Energy transfer among equivalent positions in a tetrameric protein with C4 symmetry. (*A*, *Left*) Acceptor emission intensity E_R relative to that of a single donor–acceptor pair at zero separation. E_R depends on the donor decay rate k_D and the transfer rate constant k_T, which are related to the Förster distance R_0 according to $\frac{k_D}{k_T}=\left(\frac{r}{R_0}\right)^6$. (*A*, *Center*) Assuming that the excitation intensity is well below saturation of the fluorophores (as was the case in our experiments), the combination of two donors and one acceptor yields the sum of individual FRET intensities. (*A*, *Right*) The emission from the combination of one donor and two acceptors is described by adding the two transfer rate constants. (*B*) Contributions E_R to the emission intensity from each configuration of subunits. The probability of a YFP subunit in any position is p and the corresponding CFP probability $q=1-p$. The Förster ratio is $Q=k_D/k_T$. (*C*) Energy transfer efficiency as a function of fluorophore spacing, assuming $R_0=50$ Å. The weighted sum of the E_R, normalized by the average number of YFP subunits ($4p$ in this case) gives the FRET efficiency E as defined in the main text. This is plotted as a function of nearest-neighbor distance for three values of p, representing a range of relative expression levels of the CFP and YFP subunits centered on $P=0.25$. The dotted curve (largely hidden by the $P=0.25$ curve) shows the values of E given by the fitted function: $E=\frac{1.4}{\left(\frac{0.98r}{R_0}\right)^6+1}$. The horizontal lines show the values $E=0.06$ and $E=0.5$ observed at extremes of Ca^{2+} concentration with the 667 construct.

Table S1. *G–V* fitting parameters

Parameter	BK860CY (Fig. 3*A*)	BK667CY (Fig. 4*A*)	BK667/5D5A/CY (Fig. 4*B*)	BK667/5D5A/M513I/CY (Fig. 4*C*)
V_h(J), mV	148	148	148	148
z_J, e	0.58	0.58	0.58	0.58
L_0	2.2×10^{-6}	2.2×10^{-6}	2.2×10^{-6}	2.2×10^{-6}
z_L, e	0.42	0.42	0.42	0.42
K_{d1}, μM	4.1	4.1	900	900
K_{d2}, μM	39	39	39	900
C_1	3.34	3.6	1	1
C_2	5.25	6.16	11.03	137.35
D	29.87	30.37	2.86	2.05
E_1	1	1	1	1
E_2	2.29	2.13	26.16	3.07

Column 1 (BK860CY), steady-state parameters used to compute *G–V* curves in Fig. 3*A* (*Upper*), modified from the Sweet and Cox (1) model, which is an extension of the Horrigan and Aldrich (2) model to include two Ca^{2+} binding sites. Columns 2–4 show the parameters used to compute the *G–V* curves in Fig. 4 *A–C* (*Upper*) for the BK667CY constructs indicated in the column titles. *J*, *K*, and *L* are the equilibrium constants for voltage sensor activation, Ca^{2+} binding, and C-O transition, respectively; V_h (*J*) is the voltage, where $J=1$; L_0 and z_J are the zero voltage value of *L* and its partial charge, respectively; K_{d1} and K_{d2} are the Ca^{2+} dissociation constants; and C_1, C_2, *D*, E_1, and E_2 are the allosteric constants describing channel opening/Ca^{2+} binding, channel opening/voltage sensor activation, and voltage sensor activation/Ca^{2+} binding interactions, respectively (1, 2).

1. Sweet T-B, Cox DH (2008) Measurements of the BKCa channel's high-affinity Ca^{2+} binding constants: Effects of membrane voltage. *J Gen Physiol* 132(5):491–505.
2. Horrigan FT, Aldrich RW (2002) Coupling between voltage sensor activation, Ca^{2+} binding and channel opening in large conductance (BK) potassium channels. *J Gen Physiol* 120(3): 267–305.